ACS OMEGA

Open Access

http://pubs.acs.org/journal/acsodf

Article

Synthesis and Characterization of Carbon Microbeads

Michael Jack Parente and Balaji Sitharaman*

Cite This: *ACS Omega* 2023, 8, 34034−34043

Read Online

ACCESS | Metrics & More | Article Recommendations | Supporting Information

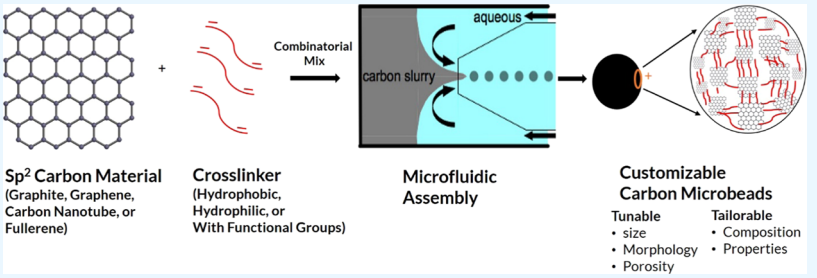

ABSTRACT: We report a microfluidic-based droplet generation platform for synthesizing micron-sized porous carbon microspheres. The setup employs carbon materials such as graphite, carbon nanotubes, graphene, fullerenes, and carbon black as starting materials. Custom composition, structure, and function are achieved through combinations of carbon materials, cross-linkers, and additives along with variations in process parameters. Carbon materials can be assembled into spheres with a mean diameter of units to hundreds of μm with relatively tight size distribution (<25% RSD). Pore structure and size (tens to hundreds of angstrom) can be modulated by incorporating porogen/coporogen dilutants during synthesis. The microbeads have excellent mechanical stability with an elastic modulus of hundreds of MPa. They can sustain high dynamic fluid flow pressures of up to 9000 psi. This work lays the foundation for synthesizing novel tailorable and customizable carbon microbeads. It opens avenues for applying these novel materials for composite and additive manufacturing, energy, life science, and biomedical applications.

INTRODUCTION

Nano-, micro-, and milliscopic spheres assembled from pristine or functionalized carbon structures (e.g., graphene, carbon nanotubes, fullerenes, natural graphite) could serve as excellent candidate materials for a wide range of applications: energy, composite additives, separation and filtration, pharmaceutical delivery, and regenerative medicine.[1,2] Over the last four decades, various methods have been explored to synthesize spherical carbon microbeads. Porous graphitic carbon compositions have been manufactured using carbon-rich molecules or polymers coated onto sacrificial inorganic templates, followed by template removal and high-temperature graphitization.[3] Liquid phase carbonization using aromatic hydrocarbons such as coal tar, heavy oil residue, and pitch has been demonstrated to form mesophase carbon beads.[4] Flame pyrolysis processes have been employed to synthesize pyrolytic graphite shells.[5−7] However, these techniques' harsh conditions (e.g., elevated temperatures) provide suboptimal or no control to tailor the bead's physiochemical properties (composition, pore size, and bead diameter).

The techniques used to produce carbon nanomaterials (e.g., graphene, carbon nanotubes, and fullerenes) have been described elsewhere.[8,9] Three-dimensional (3D) micro- and milliscopic structures using these feedstock carbon nanomaterials have been successfully assembled in the past decade.[10−25] However, the controlled synthesis of carbon spheres with micro- and milliscopic dimensions employing carbon material−binder compositions has not been demonstrated. Studies have also recognized that small molecules, oligomeric or polymeric binders may be required to process carbon materials to obtain specific physical characteristics (e.g., shapes or sizes) and physicochemical properties (e.g., mechanical, electrical) uniquely required for the above applications.[26,27] Employing these carbon material−binder compositions to synthesize carbon microspheres of various sizes in a controlled manner has not been demonstrated due to the complexity of the requirement. First, a suitable method must be developed to generate microspheres. Next, the right combination or composition of the carbon, binder, and any other additional additive(s) need to be determined, which produce mechanically stable microspheres that do not agglomerate within the constraints posed by the generation method. Finally, any additional structural (e.g., porosity) or functional (e.g., mechanical property) changes in the microspheres may require other processing steps.

Received: July 13, 2023
Accepted: August 16, 2023
Published: September 5, 2023

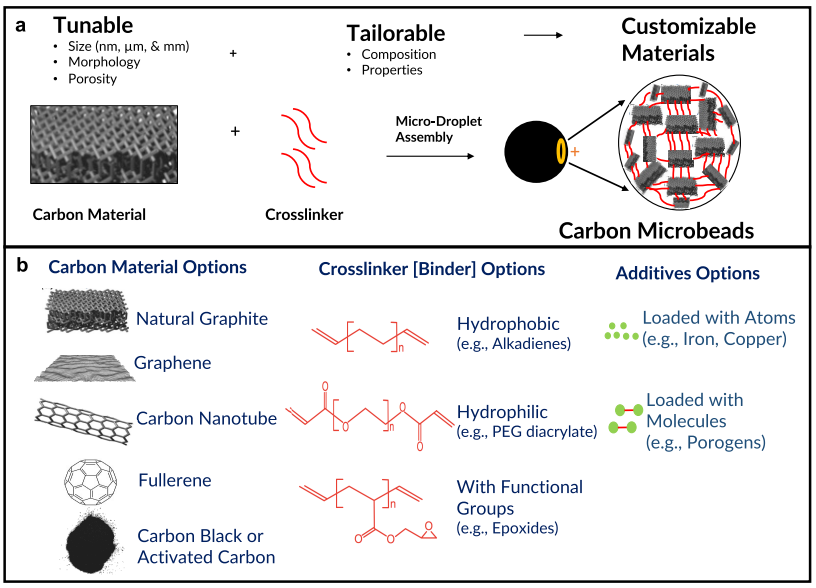

Figure 1. (a) Depiction of the customizable carbon microbead platform. Carbon sources are combined through a microdroplet assembly to create mechanically stable spheres. (b) Various feedstock inputs serve as a combinatorial library or "toolbox" to custom tailor end products with desired physical and chemical attributes.

Historically, microspheres using mainly unsaturated polymers have been synthesized employing traditional emulsion free-radical polymerization by manual or mechanical (using sonicators and homogenizers) agitation.[28] Carbon materials such as carbon black, carbon nanotubes, and graphene were used as stabilizing agents in water/oil spherical droplets known as Pickering emulsions.[29−34] Issues with these traditional methods, which include polydispersity and poor reproducibility, have led to the development of sophisticated emulsification methods like membrane extrusion, viscoelastic shear, microchannel emulsification, microthread generation, and microfluidic emulsification.[35] Spray devices (a.k.a. atomizers, applicators, sprayers, or nozzles) that discharge liquid at high velocity into a gaseous phase (usually slowly moving air) or utilize electrical or ultrasonic pressure to generate droplets have been used in material synthesis.[36−38] Indeed, the atomization technique has created microbeads employing a mix of carboxylic acid-functionalized carbon nanotubes and other additives.[39] However, these techniques provide inadequate control over the size of the microdroplets.

Microfluidic-based micron-sized droplet generation for material synthesis has emerged as a promising technique.[28,35,40] These methods allow for much higher precision and repeatability than conventional atomization techniques. Microfluidic-based droplet generation technologies have mainly been explored for low viscous dispersions to generate spherical soft gel or hydrophobic polymeric microparticles.[28,35,41,42] Commercial end-to-end microfluidic-based solutions that input viscous raw materials and output final dried products (customized to composition, density, size, shape, or porosity) are unavailable. Current commercially available technologies are unsuitable or cannot be directly adapted for viscous slurries (>200 mPa·s) of carbon materials to generate hard carbon microspheres due to the complexity of the requirements, which includes the following:

(a) Customized setup that can handle viscous carbon slurries.
(b) Customized setup for postprocessing the generated droplets into solid spheres.
(c) Additional changes in the slurry preparation and processing steps for any further structural (e.g., porosity) or functional (e.g., mechanical property) changes in the spheres.

This report presents a carbon microbead synthesis platform that addresses the above-stated challenges. This platform integrates a scalable microdroplet-based viscous slurry processing method and unique carbon material, binder, and additive combinations to generate carbon microbeads.

RESULTS AND DISCUSSION

Figure 1a presents a depiction of the carbon microbead platform. The choice of carbon materials, cross-linkers, and optional additives provide a toolbox to customize composition, structure, and function (Figure 1b). Any carbon material with carbon−carbon double bonds can be used. Thus, carbon materials such as micrographite, graphene, carbon nanotubes, and fullerenes serve as good starting materials. Carbon black and activated carbon materials with high percentages of sp^2 carbon could also be used as starting materials. Binder molecules that are either hydrophobic or hydrophilic can be used. These binders may include functional groups and may be of various lengths. A key requirement is the presence of at least one carbon−carbon double bond (preferably terminal) in these moieties. Additionally, additives could be included during synthesis. The binder and additives facilitate control over composition, structure, and function.

Figure 2a depicts a droplet generator system used to fabricate carbon microbeads. This novel system has four main components: (1) continuous phase reservoir/pressure tank, (2) syringe pump, (3) hydrophilic coflow or flow-focused nozzle, and (4) hydrophilic reaction chamber. The water-based continuous phase is loaded into the reservoir and pressurized into the tank. The flow rate and pattern of the continuous phase are controlled with the pressure regulator/pulse solenoid. The dispersed phase (carbon slurry) is loaded into

https://doi.org/10.1021/acsomega.3c05042
ACS Omega 2023, 8, 34034−34043

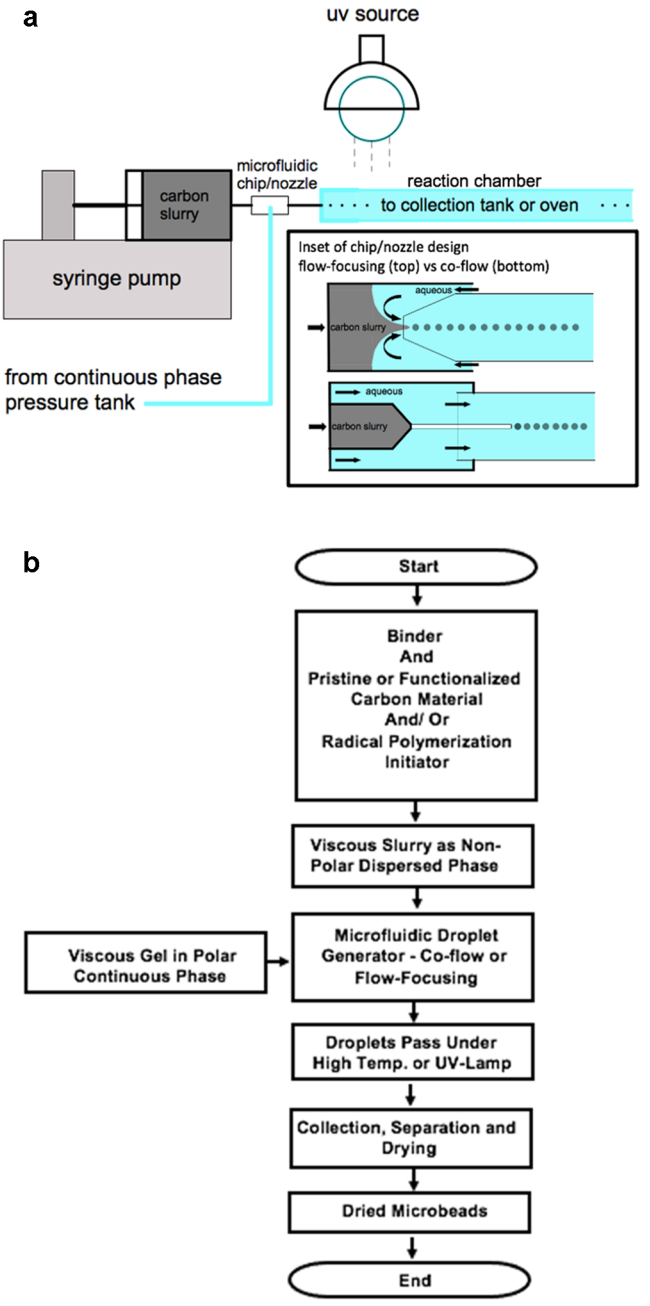

Figure 2. (a) Depiction of the synthesis setup. Inset: flow-focusing and coflow nozzle designs. A viscous suspension containing a mixture of natural carbon powder and a cross-linker (carbon slurry) is passed through a microfluidic nozzle device to generate uniform size droplets. A UV lamp facilitates the in situ binding of the mixture in microbeads. The microbeads are collected, washed, and dried. (b) Flowchart of carbon microbead synthesis steps.

a quartz capillary controlled with a syringe pump. The continuous and dispersed phases meet in the nozzle, where shear forces between the flowing immiscible fluids cause droplet snap-off. The hydrophilic surface chemistry of the nozzle ensures that the water-based continuous phase is the outer phase, keeping the hydrophobic dispersed phase as isolated drops in the center of the channel.

Figure 2b shows a flowchart of the entire carbon microbead synthesis steps. A viscous suspension (slurry) mixture of a carbon starting material and a cross-linker is passed through a microfluidic device to generate uniform size droplets. A high-temperature oven or UV lamp facilitates in situ binding of the mixture in the reaction chamber. The droplets are collected, separated, and dried. The key parameters that control the size of the microbeads are the size of the capillary tube nozzle, flow velocities, and viscosities of the two phases.

The platform (Figures 1 and 2) solves the challenge of processing high-viscosity slurries, which is needed when the carbon feedstock is in sufficiently high concentrations. When aiming to produce mechanically stable beads capable of withstanding high pressures, solid carbon content significantly increases these slurries' viscosity (>200 mPa·s). As a frame of reference, the viscosity of water is 0.89 mPa·s. The organic solvent decane and safflower oil have viscosity values of 1 and 50 mPa·s, respectively. Droplets formed using carbon dispersions in these viscosity ranges (0−50 mPa·s) have insufficient amounts of carbon materials per droplet to form mechanically stable microbeads. Droplet generation of high-viscosity solvents by others employing phase inversion techniques[43−45] has not demonstrated the capability to create droplets tailored to specific sizes.

Carbon slurry droplets are generated when two immiscible phases merge (carbon slurry is the hydrophobic phase, and the aqueous solution is the hydrophilic phase). The carbon slurry is pumped as the "inner phase" to the aqueous solution's outer phase. The droplets take a spherical conformation due to the thermodynamic principle of a minimum interfacial energy. Control over droplet formation is best achieved if the aqueous phase preferentially wets the channel walls. Thus, commercially available capillary microfluidic devices consisting of coaxial assemblies of glass capillaries on glass slides or a poly-(dimethylsiloxane) (PDMS) surface treated with hydrophilic [(polyethylene-oxy)propyl]trimethoxysilane were initially explored.[46]

Early in the design process, conventional off-the-shelf microfluidic equipment components and commercial capillary tubes were found inadequate or unsuitable and, thus, abandoned. Three key issues were noted. The first issue was the geometry of the microfluidic chip or nozzle. It could not accommodate the passage of a viscous slurry of carbon particles without clogging, while still producing droplets at the desired diameter. In the region of droplet formation, typical microfluidic chips scale down the channel width to under 100 μm in each dimension.[47,48] Standard "off-the-shelf" chips, designed as sealed chambers, did not lend to disassembly for cleaning clogged channels. Thus, custom-designed geometries using quartz glass were fabricated to address this issue.

The second issue was the volume limitations of the microfluidic continuous phase reservoir (a few hundred microliters to units of milliliters). Based on the ratio of continuous−dispersed phase volumes (50:1−300:1, depending on droplet size) required to achieve droplets in the size regime we were targeting for this highly viscous slurry, working in the scale available with off-the-shelf microfluidics equipment was not possible. Thus, a method was developed to precisely deliver the continuous phase's large volumes (hundreds of liters). The most practical solution was a large capacity tank that could be pressurized and have the fluid output controlled with a regulator and solenoid.

The third issue was that the commercial capillary tubes were unsuitable for our system. Thus, we also fabricated coflow capillary tubes of various internal diameters (300 to <20 μM). Previous studies showed that a commercially available spray

https://doi.org/10.1021/acsomega.3c05042
ACS Omega 2023, 8, 34034−34043

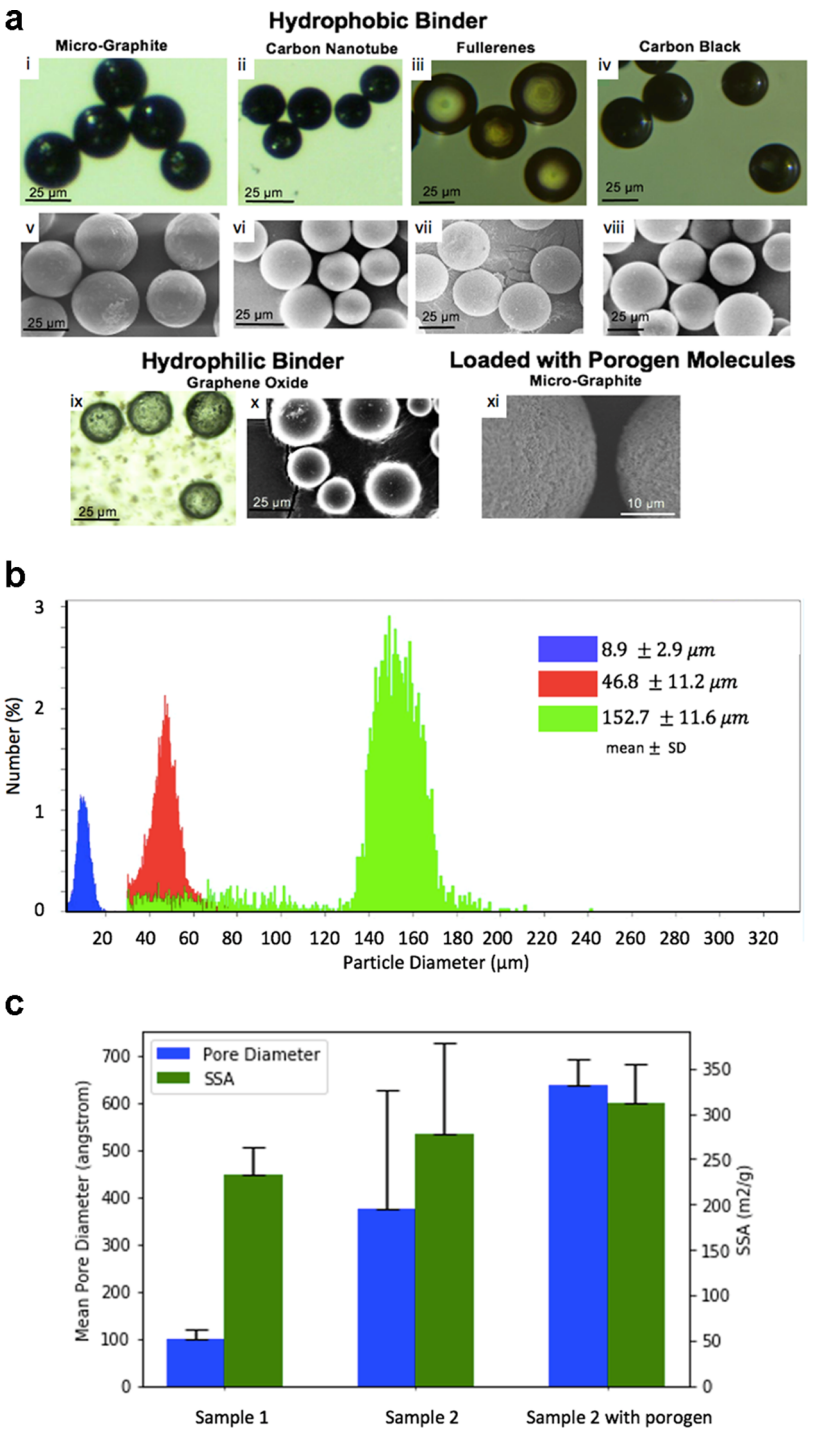

Figure 3. (a) Bright view and SEM microscopic images illustrating the spherical conformation and surface texture of carbon microbeads produced with various carbon sources. (b) Size analysis of 3 representative samples of carbon microbeads synthesized in the 10 μm (left), 50 μm (mid), and 150 μm (right) size distributions. Sample: natural graphite using the BDDMA binder. (c) Mean pore diameter and specific surface area of cured microbeads are controlled by the choice of slurry components and porogen. Sample 1: graphite with the divinylbenzene (DVB) binder. Sample 2: graphite with the 1,4-butanediol dimethacrylate (BDDMA) binder. Porogen: 1-propanol.

nozzle, which generates multiple simultaneous droplets, leads to variation in droplet size. Our customized microfluidic setup replaced these commercially available nozzles and allowed control of the size of individual droplets. Control over shear forces between the fluid phases in our coflow and flow-focusing nozzle system delivers precise control over droplet snap-off, allowing set droplet volumes.[49]

Literature review indicated that no existing theoretical modeling and experimental studies were used to predict the conditions to generate spherical droplets of a particular size using highly viscous slurries. Thus, many empirical experiments were performed due to the unpredictability and number of variables (viscosity, flow rate, surface tension, and geometric constraints). Refinement of the droplet diameter formation indicated that spherical droplets could be achieved by varying

https://doi.org/10.1021/acsomega.3c05042
ACS Omega 2023, 8, 34034−34043

the phase velocity parameters. We noted that the outer phase must flow much faster than the inner phase to produce the desired monodisperse spherical droplets. The results provided the insight that the droplet diameter and, thus, the microbead size can be controlled (decreased or increased) by modulating the phase flow velocities, modulating the viscosity of the continuous phase, and reducing the inner phase quartz capillary size.

Low-density carbon slurry droplets, once formed, are buoyant. They immediately rise in an unmodified aqueous phase, breaking apart as they reach the surface. Thus, hydrocolloids were added to modify the aqueous phase's viscosity to extend the time frame for the newly formed droplets to reach the surface. The hydrocolloids served as emulsifying agents to keep the newly formed droplets in suspended animation, resisting buoyant forces. This pause in droplet movement also provides the needed time for the carbon material−binder cross-linking process.

UV and thermal-activated techniques were investigated to cure the drops. Thermal methods were eventually pursued. We found that not all UV-activable cross-linkers could be used with carbon slurries. Instant UV-based cross-linking methods or binders that lead to quick curing for other hybrid spheres[42] did not work similarly or efficiently with carbon materials. The reason for this discrepancy is as follows. Photoinitiators used for UV curing find absorbance in the 250−400 nm spectral range. Glass filters out most of the shorter wavelengths emitted by a UV source. Optimal curing conditions require direct contact unobstructed by glass tubing, containment vessel, or specialized UV transparent materials such as fluorinated ethylene propylene (FEP)[50] or cyclic olefin copolymer (COC).[51] The black color of the carbon material slurry further added to the challenge. The slurry's opaque nature reduces the UV light's efficiency in penetrating each drop to facilitate complete curing. Thus, the right combination or composition of the carbon, binder, and any other additional additive had to be identified to obtain mechanically stable microspheres that do not agglomerate within the constraints posed by the generation method. Although heat-induced curing is a lengthy process compared to UV curing,[52,53] it alternately allows a more consistent curing protocol across the various slurry combinations.

The carbon microbead's morphology and structural (e.g., porosity) or functional (e.g., mechanical strength) properties were investigated. The morphology of the carbon microbeads was characterized by optical and scanning electronic microscopy. Figure 3a(i−iv,ix) presents bright field optical microscopy, and Figure 3a(v−viii,x,xi) shows scanning electron microscopy images of carbon microbeads synthesized using the following inputs (natural micrographite, graphene oxide, carbon nanotube, fullerene, carbon black) with hydrophobic (1,4-butanediol dimethacrylate (BDDMA)) or hydrophilic binders (poly(ethylene glycol) diacrylate). Some carbon microbeads are loaded with additives (porogen, 1-propanol, and cyclohexane) (Figure 3a(xi)). Spherically shaped mechanically stable microbeads can be synthesized from single to hundreds of microns in diameter (see Figure 3b for microbead histograms with average diameters of 10, 50, and 150 μm).

Microbead pore sizes were modulated by preparing slurries with and without using organic solvents as porogens. 1-Propanol and cyclohexane were investigated as liquid porogens due to their differences in miscibility with the liquid binder 1,4-butanediol dimethacrylate (BDDMA). The Hansen solubility parameter[54] (HSP) distance R_a^2 was calculated as 182.1 for the BDDMA−1-propanol pairing and 98.8 for the BDDMA−cyclohexane pairing. Smaller R_a^2 values indicate that the pairings are more alike and, therefore, more soluble with each other than pairing with a larger R_a^2. Studies show that pairings with greater solubility tend to create smaller pore structures. In contrast, less soluble pairings tend to generate larger pore structures.[55,56] In addition to porogens, the concentration of the carbon source, choice of the binding agent, amount of the radical initiator, polymerization times, and intensity of activation energy all factor into controlling the pore geometry. Figure 3c illustrates the controlled variation in both the pore diameter and specific surface area observed in samples of microbeads produced by altering only slurry composition parameters.

Table 1 offers a more comprehensive characterization of microbeads formed for sample 1. For this sample, a mean pore diameter of 100.3 ± 18.6 Å, a total pore volume of 0.5768 ± 0.0763 (mL/g), and a specific surface area of 233 ± 30.6 (m^2/g) were measured for carbon microbeads by water intrusion porosimetry. The same lot of beads measured using multipoint nitrogen gas adsorption isotherms applying Brunauer−Emmett−Teller (BET) analysis showed a mean pore diameter of 153.22 ± 16.55 Å, a total pore volume of 0.85 ± 0.82 (mL/g), and specific surface areas of 262.26 ± 57.59 (m^2/g) (Langmuir) and 23.62 ± 6.93 (m^2/g) (BET).

Table 1. Summary of Carbon Microbeads' Pore Diameter, Volume, and Specific Surface Area as Determined by Water Intrusion Porosimetry and BET Analysis

parameters	water intrusion porosimetry	BET analysis
mean pore diameter (Å)	100.3 ± 18.6	153.22 ± 16.55
total pore volume (mL/g)	0.5768 ± 0.0763	0.85 ± 0.82
SSA (m^2/g)	233.0 ± 30.6	262.26 ± 57.59 (Langmuir) 23.62 ± 6.93 (BET)

Mechanical properties of carbon microbeads prepared using natural micrographite as the starting material were evaluated through two different methods: (1) nanoindentation analysis of individual microbead samples and (2) backpressure analysis of fluid flow through columns packed with the microbeads. SEM imaging of the media packed in the column following the backpressure analysis was performed to assess the structural integrity and morphology of the carbon microbeads post-test.

Nanoindentation analysis performed on a sample of the carbon microbeads in the 45 μm size distribution showed the following mechanical properties: Young's modulus = 513 ± 78 MPa, reduced modulus = 587 ± 88 MPa, hardness = 304 ± 65 MPa, stiffness = 6149 ± 1377 N/m, and toughness = 130,281 ± 96,247$\sigma \times \varepsilon$, where σ is the stress in μN and ε is the strain in μM (Table 2). Additionally, the material's Poisson ratio[57] was calculated to be 0.27.

These elastic modulus values for carbon microbeads are higher than or in line with those measured for various polymeric or silica microbeads (Table S5 in the Supporting Information).

Fluid flow backpressure analysis investigated micron-sized particles' mechanical stability in a packed microbead bed, such as those found in liquid chromatography (LC) columns.[58] Previous studies have shown that if column backpressure is

https://doi.org/10.1021/acsomega.3c05042
ACS Omega 2023, 8, 34034−34043

Table 2. Summary of the Mechanical Properties of Carbon Microbeads Derived through Nanoindentation

Young's modulus	513 ± 78 MPa
reduced modulus	587 ± 88 MPa
hardness	304 ± 65 MPa
stiffness	6149 ± 1377 N/m
toughness	130,281 ± 96,247$\sigma \times \varepsilon$
poisson ratio	0.27

unstable over long-term use, it could strongly indicate a mechanical failure of the packed material.[58,59] Loading and unloading forces exerted in the high-pressure packed bed environment could fracture particles creating smaller sub-particles called fines. Column permeability can be reduced significantly by fines, causing backpressure to grow over time. Conversely, if backpressure drops abruptly, it is likely due to voids forming within the column-packed bed resulting from the breakage of the microbeads.[60,61]

The carbon microbeads packed into a 4.6 mm × 150 mm stainless steel column were subjected to significant hydraulic forces in two ways: first, in the column packing process and then through a continuous mobile phase flush for 24 h. During the packing process,[62] a slurry containing a homogenized mixture of microbeads and solvent was driven into the column under pressure to create the packed bed. A maximum force of 620 bar (9000 psi) was continuously applied to the column bed over 30 min while packing. Next, the stability test was conducted by running an isocratic mobile phase of water/acetonitrile (80:20) through the column continuously for 24 h, equating to 836 column volumes (void volume). The column void volume was determined by $V_{col} = 0.7\pi r^2 L$,[58] where r and L are the radius and length of the column, respectively. For our column, we use 1.745 mL = 1 column void volume. The criterion used to judge column stability was that backpressure ΔP showed no change of statistical significance and remained under 350 bar, similar to the published criteria.[61,63] The results indicated a stable packed bed throughout a 24 h continuous flush. The mobile phase flow rate of 1 mL/min developed a mean backpressure of 24.85 bar, showing a maximum and minimum of 25.63 and 23.81 bar, respectively (see Figure 4a). No statistical significance differences were observed in the pressure readings ($p = 0.97$).

Following the backpressure analysis, the mechanical stability of the carbon microbeads was evaluated directly through SEM imaging. The exact column used in the backpressure analysis study was disassembled, and a sample of the media nearest to the outlet frit was collected and imaged. The resulting image analysis showed no structural change to the beads and no sign of fines or other particle fragments in the unpacked column (see Figure 4b).

The microscopy, porosity, and mechanical characterization results (Figures 3 and 4) taken together indicate that the carbon microbead's composition and structural (e.g., porosity) or functional (e.g., mechanical strength) properties could be modulated through changes in the slurry preparation and processing parameters. For example, changes in microbead chemistry could be accomplished by changing the carbon type or binder chemistry (Figure 3a), and the microbead diameter could be increased or decreased (Figure 3b) by processing parameters (continuous phase flow rate). Porosity could be modulated by adding a porogen (Figure 3c). As stated above in Figure 1, the choice of carbon materials, cross-linkers, and

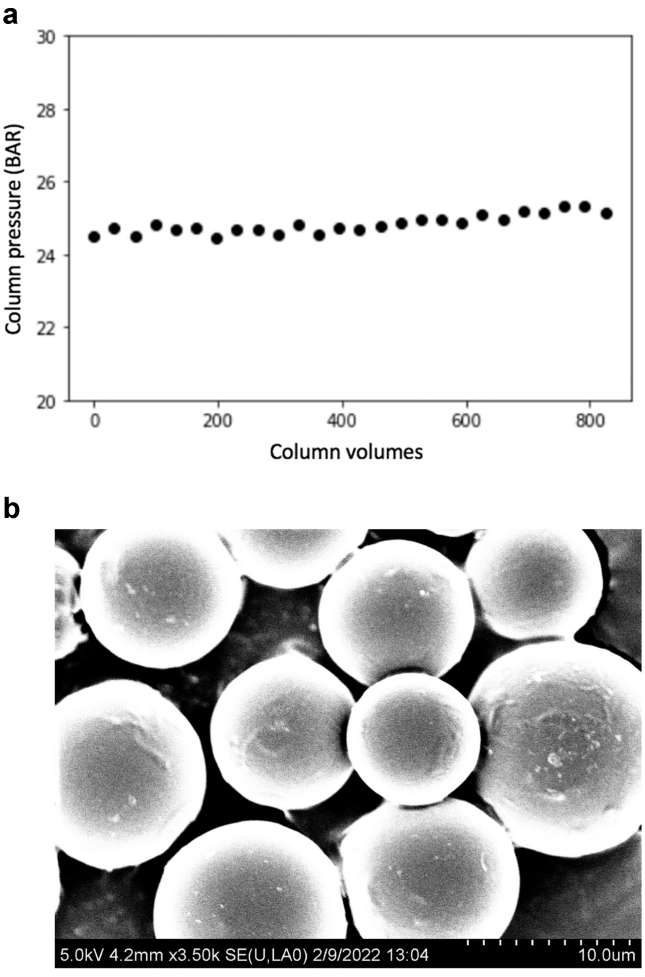

Figure 4. (a) Stability analysis. Backpressure as a function of column volumes. No statistically significant difference in backpressure was observed for the carbon microbeads packed in a liquid chromatography column for a continuous 24 h test. (b) Mechanical stability analysis. Representative SEM image of microbeads unpacked from the column after being continuously flushed for 24 h with water/acetonitrile (80:20) mobile phase. No indication of mechanical failure of the bead structure or the presence of fines in a packed bed.

optional additives provide a toolbox to customize composition, structure, and function. For instance, the porosity may also be modulated with the assistance of not only organic porogens (Figure 3c) but also other types (e.g., sodium chloride, silica, or polystyrene particles) followed by leaching of the porogen[64,65] or temperature annealing.[66,67] Additional changes in chemical properties (e.g., hydrophobicity) and/or physical properties (e.g., electrical, thermal, or magnetic properties) would require functionalization of the carbon material or incorporation of atoms or molecules into the carbon slurry (e.g., copper to modulate electrical conductivity or iron to modulate magnetic properties). Alternatively, the carbon microbead's external surface could be further functionalized through modifications.[68] Tailored sphere preparation protocols will be required to address these specific manufacturing constraints.

A key property of carbon microbeads is their excellent mechanical stability (Figure 4 and Table 2). Three-dimensional, free-standing, porous carbon structures possessing nano- and microscale-interconnected pores by radical-initiated thermal cross-linking of the sp^2 carbon bonds and annealing of

https://doi.org/10.1021/acsomega.3c05042
ACS Omega 2023, 8, 34034−34043

carbon nanostructures (fullerenes, single- and multiwalled carbon nanotubes, and graphene as the starting materials) have been developed.[2,69,70] While structures fabricated using this method exhibit structural integrity, i.e., they do not fall apart once formed, the bulk mechanical properties of these structures were not characterized. In general, these structures are brittle. Their structural integrity is insufficient for applications requiring high mechanical strength or dynamic loading and unloading forces (e.g., biomedical implants and chromatography stationary phase materials). Dynamic stresses cause fatigue due to constant loading and unloading cycles (e.g., bone in vivo or fluid flow in a chromatography column). Consequently, these structures loosen, leading to a crumbling or fragmentation. These 3D structures fabricated by the methods described above exhibit significant batch-to-batch porosity and pore size variability. The carbon microbeads overcome the above challenges. The microbeads show robust structural integrity and the ability to sustain high dynamic loading and unloading forces.

The results introduce a novel and scalable method to fabricate spherical carbon microbeads using graphite, graphene, fullerenes, carbon nanotubes, and carbon black. This method can be easily adapted to other inorganic carbon-like materials (e.g., boron nitride) or organic monomers with sp^2 carbons. Additionally, while the microbead architectures presented in this work are spherically shaped,[71] other shapes could be explored using droplet-shape-control techniques. The physiochemical results have mainly focused on microbeads synthesized by using natural graphite. Additional studies are underway to characterize and examine differences produced in the physicochemical and functional properties of microbeads synthesized using the various carbon sources described (graphite, graphene, fullerenes, carbon nanotubes, and carbon black). The findings of these additional studies should provide insights into how these physicochemical differences may be applied to energy, life science, and biomedical applications.

CONCLUSIONS

Carbon microbeads were synthesized by employing a state-of-the-art microfluidic droplet generation and processing setup that can handle highly viscous slurries. Any carbon material with sp^2 carbon networks such as graphite, carbon nanotubes, graphene, fullerenes, and sp^2 carbon-rich molecules can be used as a starting material. The inclusion of cross-linkers to bind the carbon material, along with additives and variations in process parameters, allows control over microbead's composition, size (diameter) with tunable pore structures, and surface area. The carbon beads exhibit excellent mechanical stability with the ability to withstand hydrostatic and hydrodynamic pressures up to 9000 psi. The results open avenues to synthesize novel carbon microbeads and study their functional properties for potential applications in separation sciences, energy storage, additive manufacturing, and drug delivery.

METHODS

Chemicals. The carbon sources for this work were graphite, graphene, fullerenes (C60), graphene oxide, multiwalled carbon nanotubes, and mesoporous carbon, all obtained from Sigma-Aldrich (St. Louis, MO). Additional carbon used included pristine natural graphite (Millennial Materials & Devices (India) Private Limited), graphene oxide (Theragnostic Technologies Inc.), single wall/double wall carbon, and nanotubes (Cheaptubes, Cambridgeport, VT). 1,4-Butanediol dimethacrylate, methyl methacrylate, styrene, divinylbenzene, poly(ethylene glycol) diacrylate, Luperox A98 benzoyl peroxide, 2-azobis(isobutyronitrile) 98%, 2-hydroxy-2-methyl-propiophenone, 1-propanol, cyclohexane, and 1,4-butanediol were all obtained from Sigma-Aldrich (St. Louis, MO). Xanthan gum (Bob's Red Mill), poly(vinyl alcohol) (Elvanol 71-30), and gum arabic (food grade) were purchased from Chemical Store.com. Span 80 and Hypermer were obtained from Croda (Plainsboro, NJ). Ultrapure water was sourced from a Millipore Direct Q3 UV system. Acetonitrile (HPLC grade) was purchased from Sigma-Aldrich (St. Louis, MO).

Synthesis Procedures. *Microdroplet Generator.* The custom system we developed to fabricate carbon microbeads at a pilot production scale consists of five main components: (1) continuous phase reservoir/pressure tank, (2) continuous phase pressure regulator/pulse solenoid, (3) hydrophilic coflow or flow-focused nozzle, (4) hydrophilic reaction chamber, and (5) syringe pump. The continuous and dispersed phases are directed to meet in either a coflow or flow-focusing geometry within the confines of a chamber with hydrophilic walls. Shear forces between the flowing immiscible fluids cause droplet snap-off. The hydrophilic surface chemistry of the nozzle and reaction chamber ensures that the water-based continuous phase is the "outer phase," keeping the hydrophobic carbon slurry as isolated drops in the center of the channel. Either through UV radiation or heat delivered in the reaction chamber, the materials within the newly formed droplets immediately receive activation energy to initiate cross-linking to form mechanically stable microbeads.

Carbon Slurry. The carbon slurries used to produce hard, mechanically stable carbon microbeads are formed by using at least one item each from the following groups: (1) carbon source (e.g., graphene, micrographite, carbon nanotubes, fullerenes, carbon black, etc.), (2) binder, with at least one carbon−carbon double bond (e.g., 1,4-butanediol dimethacrylate (BDDMA), styrene−divinylbenzene blends, poly(ethylene glycol) diacrylate, etc.), and (3) radical initiator (e.g., benzoyl peroxide (BP), azobis(isobutyronitrile) (AIBN), 2-hydroxy-2-methylpropiophenone, etc.). The carbon feedstock materials, radical initiator, and any additional additives (e.g., porogen, other molecules) were dispersed directly (as is) into the binder solvent and mixed using a high-speed mixer.

Continuous Phase. The microbeads produced in this investigation were formed by using a continuous phase of water with a hydrocolloid additive. These additives include but are not limited to, xanthan gum (*Xanthomonas campestris*), gum arabic (*Aacacia senegal*), poly(vinylpyrrolidone) (PVP), and poly(ethylene glycol) (PEG). Depending on the application, the additive concentration ranges from 0.05 to 5 mg/mL.

Characterization Methods. *Size Analysis.* All microbeads used in these studies were characterized by the Coulter principle using a Multisizer 4e Coulter counter (Beckman Coulter, Brea, California). The electrolyte solution used is Isoton II (Beckman Coulter). The Coulter counter was fitted with a 100 μm glass aperture to measure particles in the 2−60 μm range, a 560 μm glass aperture to measure particles in the 11−336 μm size range, and a 2000 μm glass aperture to measure particles in the 40−1200 μm size range. Microbead sample electrolyte solutions were prepared at 10% concentration (the upper operating limit of the Multisizer 4e) to yield distribution counts in the n = 50,000−100,000 range. Results

https://doi.org/10.1021/acsomega.3c05042
ACS Omega 2023, 8, 34034−34043

are reported as the mean diameter, standard deviation (SD), relative standard deviation (RSD), and d_{90}/d_{10}.

Pore Structure/SSA. Water Intrusion Porosimetry. The microbeads were characterized by an Aquapore water intrusion porosimeter: Aquapore-5k-A-1 (Porous Materials Inc. Ithaca NY). The porosimeter was operated from 15 to 5000 psi to drive water into the hydrophobic pore structure of the microbead samples. Milli Q ultrapure water was used for water intrusion. 0.5 g of dry microbead samples were used for each analysis. The results are reported as the mean pore diameter (Å), total pore volume (mL/g), and specific surface area (m^2/g).

BET. All microbeads used in these studies were characterized by a Brunauer–Emmett–Teller (BET) sorptometer: BET 201A-N-SA (Porous Materials Inc. Ithaca NY). Gas sorption analyses were conducted with N_2 (at −196 °C) as the sorbate gas. Before analysis, all samples were degassed at 80 °C in a low vacuum (~25 Pa) for 2 h to remove adsorbed species. The pore size, volume, Langmuir-specific surface area, and BET-specific surface area were calculated from 10-point N_2 adsorption isotherm analysis. BETWIN software (Porous Materials Inc. Ithaca, NY) performed all reported calculations.

Mechanical Testing. Nanoindentation. A Femto Tools FT-NMT04 in situ SEM Nanoindenter fit with a Berkovich tip, guided with an optical microscope, was used. Nanoindentation was conducted at the Center for Functional Nanomaterials, Brookhaven National Laboratory, New York. Individual microbeads were isolated and compressed multiple times, increasing the compression depth by 2 μm each until fracture. A video of the compression trials was analyzed with ImageJ software to determine each bead's lateral deformation in response to the axial compression to calculate the material's Poisson ratio v.

$$v = -\frac{\text{lateral strain}}{\text{axial strain}}$$

Young's modulus E was calculated through the relationship

$$E = \frac{1 - v^2}{\frac{1}{E_r} - \frac{1 - v_i^2}{E_i}}$$

where v is the microbead's Poisson ratio, E_r is the microbead's reduced modulus, and v_i and E_i are parameters of the nanoindentation tip. The microbead's Poisson ratio was 0.27, Berkovich tip v_i = 0.07, and Berkovich tip E_i = 1140 GPa.

The material parameters' hardness (MPa), reduced modulus (MPa), and stiffness (N/m) were directly provided by the output of the nanoindenter. Each microbead sample subjected to nanoindentation was measured multiple times (3–5), and average values were calculated.

The material toughness was found in four samples by determining the area under their stress–strain curve through numerical integration by way of the trapezoidal rule

$$\int_a^b f(x) = \sum_a^N \frac{f(x_{k-1}) + f(x_k)}{2} \cdot \Delta x_k$$

where a = 0 and b = strain value of the material rupture and $\Delta x_k = \frac{b-a}{N}$.

Hydraulic Pressure Analysis. All measurements were carried out on an Agilent 1100 HPLC system equipped with a quaternary pump, column heating compartment, degassing unit, and a variable wavelength detector model G1314A. Control and analysis were conducted with Open Lab CDS ChemStation software application v. c.01.10[201]. 4.6 mm × 150 mm stainless steel columns fitted with 0.2 μm frits (Restek) were used. The columns were packed using a Teledyne SSI, CP class column packing unit at a maximum pressure of 9000 psi.

Mechanical stability was evaluated by subjecting the microbeads to a hydraulic pressure. To achieve this, we packed samples of microbeads into stainless steel columns used for high-performance liquid chromatography. These columns were then fitted into an HPLC system to continuously pump a liquid mobile phase through the packed bed at pressures up to 350 bar (5076 psi) for 836 column volumes. For the duration of each run, column backpressure was monitored by the HPLC system (mobile phase A: ultrapure water, mobile phase B: acetonitrile, gradient: isocratic at 20%B, flow rate: 1 mL/min, column temperature: 25 °C)

The column volume was determined by

$$V_{col} = 0.7\pi r^2 L$$

where r and L are the radius and length of the column, respectively.[72]

Image Analysis. Optical Microscopy. All microbeads used in these studies were characterized by an OMAX optical microscope model M837ZL-C180U3 40X-2500X fitted with an 18-megapixel camera model A35180U3. OMAX Toupview software application 3.7 was used for image analysis. Small quantities of dry microbeads were placed on the surface of the glass slides. Next, slides were held on the edge to pour the microbeads off and gently tapped. Excess layers of microbeads were removed by gravity and tapping, leaving only a fine monolayer of beads behind. Slides with a monolayer of microbeads remaining were directly applied to the microscope and imaged with 10× and 40× objective lenses.

SEM. SEM imaging was performed on a Hitachi 4800 scanning electron microscope at the Center for Functional Nanomaterials, Brookhaven National Laboratory, New York. Images were generated with an accelerating voltage of 5 kV and an emission current of 10 μA. Microbead samples were mounted on 2 in. sample pucks (Ted Pella Inc.) using double-sided adhesive carbon conductive tabs (PELCO Tabs). Before imaging, each sample was sputter-coated with a 7 nm thick layer of gold.

Statistical Analysis. Statistical analysis was performed using Student's t test and one-way ANOVA followed by Tukey Kramer post hoc analysis. A 95% confidence interval ($p < 0.05$) was used for all statistical analyses.

■ ASSOCIATED CONTENT

Supporting Information

The Supporting Information is available free of charge at https://pubs.acs.org/doi/10.1021/acsomega.3c05042.

Experimental data for water intrusion porosimetry, BET, and nanoindentation analysis and Young's modulus of the beads produced in this work alongside other similar materials (PDF)

■ AUTHOR INFORMATION

Corresponding Author

Balaji Sitharaman − *Millennial Scientific, Stony Brook, New York 11790, United States;* orcid.org/0000-0001-8391-

https://doi.org/10.1021/acsomega.3c05042
ACS Omega 2023, 8, 34034−34043

8076; Phone: +1-855-388-2800; Email: balaji@millennialscientific.com

Author

Michael Jack Parente − *Millennial Scientific, Stony Brook, New York 11790, United States*

Complete contact information is available at: https://pubs.acs.org/10.1021/acsomega.3c05042

Author Contributions

M.J.P. conceptualized, designed, and performed the experiments, analyzed the data, and wrote the paper; B.S. conceptualized the experiments, analyzed the data, and wrote the paper.

Notes

The authors declare the following competing financial interest(s): Millennial Scientific and the investigators have filed patents. They are developing commercial products related to the technology reported in this article.

■ ACKNOWLEDGMENTS

The National Institutes of Health (1R43AT010583 and 1R44AT012008) and the National Science Foundation (1746697 and 1926852) supported the work. This research used resources of the Center for Functional Nanomaterials Materials Characterization facility, which is of the U.S. DOE Office of Science Facilities at Brookhaven National Laboratory under Contract No. DE-SC0012704. We appreciate the assistance of Dr. Aaron Michelson with nanoindentation and Kim Kisslinger and Gwen Wright for guidance with sputter-coating and SEM operation.

■ REFERENCES

(1) Deng, X.; Li, J.; Ma, L.; Sha, J.; Zhao, N. Three-dimensional porous carbon materials and their composites as electrodes for electrochemical energy storage systems. *Mater. Chem. Front.* **2019**, *3* (11), 2221−2245.

(2) Lalwani, G.; Patel, S. C.; Sitharaman, B. Two- and Three-Dimensional All-Carbon Nanomaterial Assemblies for Tissue Engineering and Regenerative Medicine. *Ann. Biomed. Eng.* **2016**, *44* (6), 2020−2035.

(3) Knox, J. H.; Gilbert, M. T. Preparation of Porous Carbon. U.S. Patent US4,263,268A, 1981.

(4) Lü, Y.; Ling, L.; Wu, D.; Liu, L.; Zhang, B.; Mochida, I. Preparation of mesocarbon microbeads from coal tar. *J. Mater. Sci.* **1999**, *34* (16), 4043−4050.

(5) Grass, R.; Athanassiou, E.; Stark, W. Methods and Devices for Flame Spray Pyrolysis. U.S. Patent US8,182,573, 2012.

(6) Lu, A.-H.; Li, W.-C.; Matoussevitch, N.; Spliethoff, B.; Bönnemann, H.; Schüth, F. Highly stable carbon-protected cobalt nanoparticles and graphite shells. *Chem. Commun.* **2005**, No. 1, 98−100.

(7) Grass, R. N.; Stark, W. J. Carbon Coated Magnetic Nanoparticles and Their Use in Separation Processes. U.S. Patent US8801936B2, 2014.

(8) Speranza, G. Carbon nanomaterials: Synthesis, functionalization and sensing applications. *Nanomaterials* **2021**, *11* (4), 967.

(9) Onyancha, R. B.; Ukhurebor, K. E.; Aigbe, U. O.; Osibote, O. A.; Kusuma, H. S.; Darmokoesoemo, H. A methodical review on carbon-based nanomaterials in energy-related applications. *Adsorpt. Sci. Technol.* **2022**, *2022*, 1−21.

(10) Huang, J. Q.; Zhang, Q.; Zhao, M. Q.; Xu, G. H.; Wei, F. Patterning of hydrophobic three-dimensional carbon nanotube architectures by a pattern transfer approach. *Nanoscale* **2010**, *2* (8), 1401−1404.

(11) Ren, Z. F.; Huang, Z. P.; Xu, J. W.; Wang, J. H.; Bush, P.; Siegal, M. P.; Provencio, P. N. Synthesis of large arrays of well-aligned carbon nanotubes on glass. *Science* **1998**, *282* (5391), 1105−1107.

(12) Bennett, R. D.; Hart, A. J.; Miller, A. C.; Hammond, P. T.; Irvine, D. J.; Cohen, R. E. Creating patterned carbon nanotube catalysts through the microcontact printing of block copolymer micellar thin films. *Langmuir* **2006**, *22* (20), 8273−8276.

(13) De Volder, M.; Tawfick, S. H.; Park, S. J.; Copic, D.; Zhao, Z.; Lu, W.; Hart, A. J. Diverse 3D microarchitectures made by capillary forming of carbon nanotubes. *Adv. Mater.* **2010**, *22* (39), 4384−4389.

(14) Qu, J.; Zhao, Z.; Wang, X.; Qiu, J. Tailoring of three-dimensional carbon nanotube architectures by coupling capillarity-induced assembly with multiple CVD growth. *J. Mater. Chem.* **2011**, *21* (16), 5967 DOI: 10.1039/c0jm03326j.

(15) Chakrapani, N.; Wei, B.; Carrillo, A.; Ajayan, P. M.; Kane, R. S. Capillarity-driven assembly of two-dimensional cellular carbon nanotube foams. *Proc. Natl. Acad. Sci. U.S.A.* **2004**, *101* (12), 4009−4012.

(16) Endo, M.; Muramatsu, H.; Hayashi, T.; Kim, Y. A.; Terrones, M.; Dresselhaus, M. S. Nanotechnology: 'buckypaper' from coaxial nanotubes. *Nature* **2005**, *433* (7025), 476.

(17) Cao, A.; Dickrell, P. L.; Sawyer, W. G.; Ghasemi-Nejhad, M. N.; Ajayan, P. M. Super-compressible foamlike carbon nanotube films. *Science* **2005**, *310* (5752), 1307−1310.

(18) Xu, M.; Futaba, D. N.; Yamada, T.; Yumura, M.; Hata, K. Carbon nanotubes with temperature-invariant viscoelasticity from −196 degrees to 1000 degrees C. *Science* **2010**, *330* (6009), 1364−1368.

(19) Gui, X.; Wei, J.; Wang, K.; Cao, A.; Zhu, H.; Jia, Y.; Shu, Q.; Wu, D. Carbon nanotube sponges. *Adv. Mater.* **2010**, *22* (5), 617−621.

(20) Worsley, M. A.; Kucheyev, S. O.; Satcher, J. J. H.; Hamza, A. V.; Baumann, T. F. Mechanically robust and electrically conductive carbon nanotube foams. *Appl. Phys. Lett.* **2009**, *94* (7), No. 073115.

(21) Kim, K. H.; Oh, Y.; Islam, M. F. Graphene coating makes carbon nanotube aerogels superelastic and resistant to fatigue. *Nat. Nanotechnol.* **2012**, *7* (9), 562−566.

(22) Schiffres, S. N.; Kim, K. H.; Hu, L.; McGaughey, A. J. H.; Islam, M. F.; Malen, J. A. Gas Diffusion, Energy Transport, and Thermal Accommodation in Single-Walled Carbon Nanotube Aerogels. *Adv. Funct. Mater.* **2012**, *22*, 5251−5258.

(23) Worsley, M. A.; Pauzauskie, P. J.; Olson, T. Y.; Biener, J.; Satcher, J. H.; Baumann, T. F. Synthesis of Graphene Aerogel with High Electrical Conductivity. *J. Am. Chem. Soc.* **2010**, *132* (40), 14067−14069.

(24) Zhang, X.; Sui, Z.; Xu, B.; Yue, S.; Luo, Y.; Zhan, W.; Liu, B. Mechanically strong and highly conductive graphene aerogel and its use as electrodes for electrochemical power sources. *J. Mater. Chem.* **2011**, *21* (18), 6494−6497.

(25) Biener, J.; Stadermann, M.; Suss, M.; Worsley, M. A.; Biener, M. M.; Rose, K. A.; Baumann, T. F. Advanced carbon aerogels for energy applications. *Energy Environ. Sci.* **2011**, *4* (3), 656−667.

(26) Bosnyak, C. P.; Swogger, K. W.; Marinkovic, M. Binders, electrolytes and separator films for energy storage and collection devices using discrete carbon nanotubes. US10608282B22013.

(27) Belmont, J. A.; Johnson, J. E.; Adams, C. F. Ink Jet Ink Formulations Containing Modified Carbon Products. U.S. Patent US5,630,868, 1995.

(28) Choi, A.; Seo, K. D.; Kim, D. W.; Kim, B. C.; Kim, D. S. Recent advances in engineering microparticles and their nascent utilization in biomedical delivery and diagnostic applications. *Lab Chip* **2017**, *17* (4), 591−613.

(29) Adamson, D. H.; Woltornist, S.; Dobrynin, A. V. Graphene/Graphite Polymer Composite Foam Derived from Emulsions Stabilized by Graphene Kinetic Trapping. U.S. Patent US20170178762A1, 2014.

(30) Woltornist, S. J.; Carrillo, J.-M. Y.; Xu, T. O.; Dobrynin, A. V.; Adamson, D. H. Polymer/Pristine Graphene Based Composites:

From Emulsions to Strong, Electrically Conducting Foams. *Macromolecules* **2015**, *48* (3), 687−693.
(31) Song, X.; Yang, Y.; Liu, J.; Zhao, H. PS Colloidal Particles Stabilized by Graphene Oxide. *Langmuir* **2011**, *27* (3), 1186−1191.
(32) Kim, J.; Cote, L. J.; Kim, F.; Yuan, W.; Shull, K. R.; Huang, J. Graphene Oxide Sheets at Interfaces. *J. Am. Chem. Soc.* **2010**, *132* (23), 8180−8186.
(33) Wang, H.; Hobbie, E. K. Amphiphobic Carbon Nanotubes as Macroemulsion Surfactants. *Langmuir* **2003**, *19* (8), 3091−3093.
(34) Nikova, A. T.; Bose, A.; Sharma, R. Porous Carbon Monoliths Templated by Pickering Emulsions. WO2014070987A1, 2012.
(35) Shah, R. K.; Shum, H. C.; Rowat, A. C.; Lee, D.; Agresti, J. J.; Utada, A. S.; Chu, L.-Y.; Kim, J.-W.; Fernandez-Nieves, A.; Martinez, C. J.; Weitz, D. A. Designer emulsions using microfluidics. *Mater. Today* **2008**, *11* (4), 18−27.
(36) D'Addio, S. M.; Chan, J. G. Y.; Kwok, P. C. L.; Benson, B. R.; Prud'homme, R. K.; Chan, H.-K. Aerosol Delivery of Nanoparticles in Uniform Mannitol Carriers Formulated by Ultrasonic Spray Freeze Drying. *Pharm. Res.* **2013**, *30* (11), 2891−2901.
(37) Taksima, T.; Limpawattana, M.; Klaypradit, W. Astaxanthin encapsulated in beads using ultrasonic atomizer and application in yogurt as evaluated by consumer sensory profile. *LWT–Food Sci. Technol.* **2015**, *62* (1, Part 2), 431−437.
(38) Scattergood, J. R. Atomization Technique for Producing Fine Particles. U.S. Patent US7,131,597B2, 2003.
(39) Liguo, S.; Xiaoyu, C.; Xiaoyu, S.; Cheng, W.; Yanhong, Z. Method for Manufacturing Carbon Nano Tube Micro Beads. CN104525070A, 2015.
(40) Visser, C. W.; Kamperman, T.; Karbaat, L. P.; Lohse, D.; Karperien, M. In-air microfluidics enables rapid fabrication of emulsions, suspensions, and 3D modular (bio)materials. *Sci. Adv.* **2018**, *4* (1), No. eaao1175.
(41) Chu, L.-Y.; Kim, J.-W.; Shah, R. K.; Weitz, D. A. Monodisperse Thermoresponsive Microgels with Tunable Volume-Phase Transition Kinetics. *Adv. Funct. Mater.* **2007**, *17* (17), 3499−3504.
(42) Kim, D.-Y.; Jin, S. H.; Jeong, S.-G.; Lee, B.; Kang, K.-K.; Lee, C.-S. Microfluidic preparation of monodisperse polymeric microspheres coated with silica nanoparticles. *Sci. Rep.* **2018**, *8* (1), No. 8525.
(43) Man, J.; Li, Z.; Li, J.; Chen, H. Phase inversion of slug flow on step surface to form high viscosity droplets in microchannel. *Appl. Phys. Lett.* **2017**, *110* (18), No. 181601.
(44) Chen, H.; Man, J.; Li, Z.; Li, J. Microfluidic Generation of High-Viscosity Droplets by Surface-Controlled Breakup of Segment Flow. *ACS Appl. Mater. Interfaces* **2017**, *9* (25), 21059−21064.
(45) Au - Li, J.; Au - Man, J.; Au - Li, Z.; Au - Chen, H. Fabricating High-viscosity Droplets using Microfluidic Capillary Device with Phase-inversion Co-flow Structure. *JoVE* **2018**, *134*, No. e57313.
(46) Shah, R. K.; Shum, H. C.; Rowat, A. C.; Lee, D.; Agresti, J. J.; Utada, A. S.; Chu, L.-Y.; Kim, J.-W.; Fernandez-Nieves, A.; Martinez, C. J.; Weitz, D. A. Designer emulsions using microfluidics. *Mater. Today* **2008**, *11* (4), 18−27.
(47) Thorsen, T.; Roberts, R. W.; Arnold, F. H.; Quake, S. R. Dynamic pattern formation in a vesicle-generating microfluidic device. *Phys. Rev. Lett.* **2001**, *86* (18), 4163.
(48) Anna, S. L. Droplets and bubbles in microfluidic devices. *Annu. Rev. Fluid Mech.* **2016**, *48*, 285−309.
(49) Tan, Y.-C.; Cristini, V.; Lee, A. P. Monodispersed microfluidic droplet generation by shear focusing microfluidic device. *Sens. Actuators, B* **2006**, *114* (1), 350−356.
(50) Evenhuis, C. J.; Yang, W. C.; Johns, C.; Macka, M.; Haddad, P. R. Fluorinated ethylenepropylene copolymer as a potential capillary material in CE. *Electrophoresis* **2007**, *28* (19), 3477−3484.
(51) Bruijns, B.; Veciana, A.; Tiggelaar, R.; Gardeniers, H. Cyclic olefin copolymer microfluidic devices for forensic applications. *Biosensors* **2019**, *9* (3), 85.
(52) Hui, A. W.; Hamielec, A. E. Thermal polymerization of styrene at high conversions and temperatures. An experimental study. *J. Appl. Polym. Sci.* **1972**, *16* (3), 749−769.
(53) Ručigaj, A.; Alič, B.; Krajnc, M.; Šebenik, U. Curing of bisphenol A-aniline based benzoxazine using phenolic, amino and mercapto accelerators. *eXPRESS Polym. Lett.* **2015**, *9* (7), 647−657, DOI: 10.3144/expresspolymlett.2015.60.
(54) Hansen, C. *The Three Dimensional Solubility Parameter and Solvent Diffusion Coefficient and Their Importance in Surface Coating Formulation*, Danish Technical Press: Copenhagen, 1967.
(55) Yu, S.; Ng, F. L.; Ma, K. C. C.; Mon, A. A.; Ng, F. L.; Ng, Y. Y. Effect of porogenic solvent on the porous properties of polymer monoliths. *J. Appl. Polym. Sci.* **2013**, *127* (4), 2641−2647.
(56) Mohamed, M. H.; Wilson, L. D. Porous copolymer resins: tuning pore structure and surface area with non reactive porogens. *Nanomaterials* **2012**, *2* (2), 163−186.
(57) Singaravelu, A. S. S.; Williams, J. J.; Shevchenko, P.; Ruppert, J.; De Carlo, F.; Henderson, M.; Holmes, C.; Chawla, N. Poisson's ratio of eTPU molded bead foams in compression via in situ synchrotron X-ray microtomography. *J. Mater. Sci.* **2021**, *56* (22), 12920−12935.
(58) Kazakevich, Y.; Lobrutto, R.*HPLC for Pharmaceutical Scientists*; John Wiley & Sons, 2006; pp 445−447.
(59) LoBrutto, R.; A., J; Jones, A.; Prowse, T.; Vivilecchia, R. In *UPLC- A Critical Look at System/Column Performance and Method Transfer Considerations for Pharmaceutical Analytes*, HPLC 2005, Stockholm Sweden, Stockholm Sweden, 2005.
(60) Claessens, H. A.; van Straten, M. A.; Kirkland, J. J. Effect of buffers on silica-based column stability in reversed-phase high-performance liquid chromatography. *J. Chromatogr. A* **1996**, *728* (1), 259−270.
(61) Ye, C.; Terfloth, G.; Li, Y.; Kord, A. A systematic stability evaluation of analytical RP-HPLC columns. *J. Pharm. Biomed. Anal.* **2009**, *50* (3), 426−431.
(62) SSI, T., Start-Up Guid Constant Pressure Column Packing System. www.teledynessi.com, 2018.
(63) Kirkland, J.; Henderson, J.; DeStefano, J.; Van Straten, M.; Claessens, H. Stability of silica-based, endcapped columns with pH 7 and 11 mobile phases for reversed-phase high-performance liquid chromatography. *J. Chromatogr. A* **1997**, *762* (1−2), 97−112.
(64) Ma, P. X. Reverse Fabrication of Porous Materials. WO2001087575, 2001.
(65) Haugan, E.; Granlund, H.; Gjessing, J.; Marstein, E. S. Colloidal Crystals as Templates for Light Harvesting Structures in Solar Cells. *Energy Procedia* **2011**, *10*, 292−296.
(66) Striemer, C. C.; Gaborski, T. R.; McGrath, J. L.; Fauchet, P. M. Charge- and size-based separation of macromolecules using ultrathin silicon membranes. *Nature* **2007**, *445*, 749.
(67) Striemer, C. C.; Fauchet, P. M.; Gaborski, T. R.; McGrath, J. L. Ultrathin Porous Nanoscale Membranes, Methods of Making, and Uses Thereof. U.S. Patent US8,182,590, 2006.
(68) Di Giovannantonio, M.; Kosmala, T.; Bonanni, B.; Serrano, G.; Zema, N.; Turchini, S.; Catone, D.; Wandelt, K.; Pasini, D.; Contini, G.; Goletti, C. Surface− Enhanced Polymerization via Schiff-Base Coupling at the Solid−Water Interface under pH Control. *J. Phys. Chem. C* **2015**, *119* (33), 19228−19235.
(69) Lalwani, G.; Kwaczala, A. T.; Kanakia, S.; Patel, S. C.; Judex, S.; Sitharaman, B. Fabrication and characterization of three-dimensional macroscopic all-carbon scaffolds. *Carbon* **2013**, *53*, 90−100.
(70) Patel, S. C.; Lalwani, G.; Grover, K.; Qin, Y.-X.; Sitharaman, B. Fabrication and Cytocompatibility of In Situ Crosslinked Carbon Nanomaterial Films. *Sci. Rep.* **2015**, *5*, No. 10261.
(71) Gao, Y.; Zhao, C.-X.; Sainsbury, F. Droplet shape control using microfluidics and designer biosurfactants. *J. Colloid Interface Sci.* **2021**, *584*, 528−538.
(72) Kazakevich, Y.; Lobrutto, R.*HPLC for Pharmaceutical Scientists*; Wiley, 2007; pp 263−279.

https://doi.org/10.1021/acsomega.3c05042
ACS Omega 2023, 8, 34034−34043